Title: Effect of high temperature thermal treatment on the electrochemical performance of natural flake graphite

Journal of MATERIALS RESEARCH

Article
DOI:10.1557/s43578-024-01282-z

Effect of high temperature thermal treatment on the electrochemical performance of natural flake graphite

Anna Lähde[1,a], Juho Välikangas[2,3], Arūnas Meščeriakovas[1], Tommi Karhunen[1], Sara-Maaria Meščeriakovė[1], Olli Sippula[1,4], Seppo Leinonen[5], Ulla Lassi[2,3], Jorma Jokiniemi[1]

[1] Fine Particle and Aerosol Technology Laboratory, Department of Biological and Environmental Sciences, University of Eastern Finland, P.O. Box 1627, 70211 Kuopio, Finland
[2] Research Unit of Sustainable Chemistry, University of Oulu, P.O. Box 8000, 90014 Oulu, Finland
[3] Kokkola University Consortium Chydenius, University of Jyvaskyla, P.O. Box 567, 67100 Kokkola, Finland
[4] Department of Chemistry, University of Eastern Finland, P.O. Box 111, 89010 Joensuu, Finland
[5] Geological Survey of Finland (GTK), Neulaniementie 5, 70211 Kuopio, Finland
[a] Address all correspondence to this author. e-mail: anna.lahde@uef.fi

Received: 8 September 2023; accepted: 2 January 2024

Natural graphite is currently considered as a critical raw material in EU. The demand for graphite is still increasing as it is commonly used in the anodes of the Li-ion batteries (LIBs). The total graphite content for energy storage applications such as LIBs should be more than 99.95%. Several purification processes for natural graphite exist but the requirement of high purity is challenging. Here we present the high temperature thermal treatment for natural graphite ores. Thermal treatment at 2400 °C for 15 min can produce battery-grade graphite with high purity and crystallinity needed for the optimum performance of the battery cells. In addition, the crystallinity and crystalline structure of graphite was improved during the treatment. The electrochemical studies of thermally treated graphite powders showed increased electrochemical performance compared to the untreated graphite samples. The improved performance was attributed to the increased purity and crystallinity of the thermally treated powders.

Abbreviations

CRM	Critical raw material
DL	Detection limit
EDS	Energy-dispersive X-ray spectroscopy
FWHM	Full width half maximum value
G	Pristine graphite powder
G-2400	Pristine graphite powder treated at 2400 °C
G-M	Medium fraction of flotation pre-treated graphite
G-M-2400	Flotation pre-treated graphite treated at 2400 °C
GTK	Geological Survey of Finland GTK
HOPG	Highly ordered pyrolytic graphite
ICP-MS	Inductively coupled plasma mass spectrometry
LIB	Li-ion battery
MIBC	Methyl Isobutyl Carbinol
n.a.	Not applicable
NCM	$LiNi_{0.88}Co_{0.9}Mn_{0.3}O_2$
SEI	Solid electrolyte interphase
SEM	Scanning electron microscope
TGA	Thermogravimetric analyzer
TGC	Total graphitic carbon
XRD	X-Ray diffraction

Introduction

Graphite is a carbon allotrope which consists of stacked sp^2-hybridized C_6 rings. It exists in several polymorphic forms including rhombo-hedral, hexagonal, and turbostratic structures [1] graphite is considered as a critical raw material (CRM) in EU as it is widely used in number of applications and products such as Li-ion batteries (LIBs), supercapacitors, refractory materials, steel production, due to its excellent physico-chemical properties [2–5]. China is currently the leading producer of natural graphite followed by India and Brazil [3]. The total natural graphite production in the world was around one million tons in 2021 [6] and the demand of natural graphite is expected to

increase significantly in the upcoming years due to the increasing demand of LIBs [3].

Graphite can be obtained either from natural ores by mining or it can be produced synthetically [1, 3]. Natural graphite is an earth-abundant carbon material that can be classified into the following categories: (i) flake graphite, (ii) lump graphite, and iii) amorphous graphite [2]. Amorphous graphite is the most abundant in nature and it consists of very fine graphite particles. However, its purity is only around 70 to 85% even after the processing, while the purity of flake graphite, for example, can be increased to over 90%. This is still far below the purity required for LIBs [2, 3].

There are several different chemical and thermal methods for the purification of natural graphite including hydrometallurgical and pyrometallurgical processes, comminution, froth flotation [3, 6, 7]. The degree of purity and crystalline structure of the obtained natural graphite is dependent on the chosen purification method. However, most methods typically contain several stages, are time consuming and use toxic chemicals causing environmental hazards.

Highly ordered pyrolytic graphite (HOPG) can be synthesized from the fossil-based precursors such as petroleum coke or coal tar pitch at high temperatures between 2500 and 3000 °C with holding time of several hours [8–10]. HOPG has very small amounts of impurities and it is the main form of graphite used in LIB anode materials where high purity graphite is required [8]. However, the production of synthetic graphite is more expensive than natural graphite and alternative options for highly pure, ordered graphite are needed. Thus, new, environmentally friendly, and cost-effective purification and crystallization technologies of the natural graphite are needed to reach the requirements of the battery grade graphite.

For energy storage applications such as LIBs the total graphite content should be more than 99.95% [2, 3], thus synthetic graphite made from fossil precursors is still mostly used in electrode material. The flake size for the battery applications varies typically from 100 µm to 300 µm. In addition, highly crystalline 2H-graphite is preferred over other crystalline structures (e.g., turbostratic graphite, hard graphite) to achieve optimum intercalation of lithium (LiC_6) for a near theoretical capacity of 372 mAh/g [11].

Here we present the thermal purification method for natural flake graphite obtained from Aitolampi, Finland. The graphite ore was previously treated with a flotation method and divided to large (> 180 µm), medium (75–180 µm), and fine particle (< 75 µm) fractions. The medium size fraction, which is in the size range typically used for battery applications, was used for thermal treatment purification, crystallization, and electrochemical studies presented in this paper. The thermal treatment was carried out by utilizing induction annealing, which is a highly efficient heating method with transferable heat over several times higher compared to the conventional joule heating [12]. The graphite samples were subjected to high temperature (2400 °C) under argon atmosphere at atmospheric pressure between five and fifteen minutes. Besides the relatively short time under the high temperature compared, for example, to the production of synthetic graphite, high purity above 99.8% and increased crystallinity of the natural graphite was obtained. The purity, crystalline structure and morphology of the produced graphite was analyzed before and after the thermal treatment with electron microscopy, Raman, ICP-MS, and XRD. Finally, electrochemical studies of the thermally treated graphite powders were carried out and compared to the untreated samples showing the improved capacity and cycle of the thermally purified samples.

Results and discussion

Thermal purification of the graphite powders

The impurities in natural graphite originating from Aitolampi deposit were analyzed with ICP-MS, see Table 1. The most important impurities of the pristine, untreated graphite samples (sample G) were iron (73 171 µg/g), aluminum (42 569 µg/g), silicon (245 458 µg/g), and potassium (20 484 µg/g). In addition to these elements, the untreated samples also contained sodium, calcium, and magnesium above 10 000 µg/g. These impurities were partly removed with the conventional flotation (see sample G-M in Table 1). However, there were still relatively high amounts of silicon, aluminum, and iron left in the samples, which makes these powders unsuitable for the Li-ion electrode applications in which the total graphite content should be very high [2, 3].

Thermodynamic equilibrium calculations were carried out to estimate the vaporization temperatures of the main contaminants in the natural graphite. The results indicate that most of the impurities can be efficiently removed already below 2400 °C

TABLE 1: ICP-MS analysis of the untreated, pristine graphite powders (G), flotation treated powders (G-M), and G and G-M powders treated at 2400 °C for 15 min (G-2400, G-M-2400, respectively).

Sample	Na (µg/g)	Mg (µg/g)	Al (µg/g)	Si (µg/g)	K (µg/g)	Ca (µg/g)	Fe (µg/g)	Zn (µg/g)	V (µg/g)
G	14,521	12,733	42,569	245,458	20,484	18,375	73,171	3016	1136 31
G-2400	< DL	36	63	< DL	63	< DL	7673	112	3934 33
G-M100	2289	4906	10,577	72	4930	85	128	85	128
G-M-2400	< DL	24	180	< DL	220	471	1521	61	5.5

at inert atmosphere with the continuous gas flow around the powder sample, see Fig. 1. First, magnesium is estimated to be vaporized already at about 1200 °C due to the decomposition of magnesium-containing silicates. Second, aluminum vaporizes below 1500 °C when aluminum oxides become thermally unstable. Third, iron vaporizes below 1700 °C as FeSi becomes thermally unstable. Finally, silicon is estimated to vaporize below 2200 °C by decomposition of SiC, while most of the carbon still remains in the solid phase. It should be noted that these results are theoretical estimates of graphite heating process without assuming imperfect mixing, reaction kinetic limitations and heterogeneous process conditions, which likely occur in the real experimental system. Therefore, the results are indicative and require verification by experiments. Thus, based on the obtained results, the thermal purification by induction heating of pristine graphite sample (sample G) and the sample pre-treated with flotation (sample G-M) was carried out at 2400 °C.

Three different holding times (5, 10, and 15 min) for thermal treatment were tested (see Supplementary Table ST1). According to the results, the thermal treatment by induction process applied for 15 min was sufficient to remove most impurities from natural graphite, see Table 1. Thermal treatment of the pristine graphite sample G showed a considerable total mass loss at 2400 °C, which is consistent with the initial low graphite content (5.1 wt-%). Thus, the pre-treatment that produces graphite concentrate significantly reduces the amount of the powders needed to be handled in thermal purification. For pre-treated samples (G-M), the thermal treatment decreased the amount of most impurities below 1000 µg/g which is in good agreement with thermodynamic calculations. The only exception was iron, which concentration remained at 1521 µg/g, see Table 1. This indicates that there are still some iron compounds in the sample that were not taken into account in the calculations. However, it should be noted that the total iron concentration remaining in the sample was relatively low as the results show micrograms in a gram of the sample.

DL detection limit

Figure 2(a) shows the thermogravimetric analysis of the flotation treated and thermally purified samples, which are in good agreement with the calculations and ICP-MS (Table 1) and the SEM/EDS (Fig. S1) analysis results. TGA result of flotation treated G-M sample [Fig. 2(a)] displayed a mass loss of 93.13%, while the remaining mass (6.87%) indicated presence of impurities. These impurities were composed of Si, Fe, Na, S, Ca, Mg, K

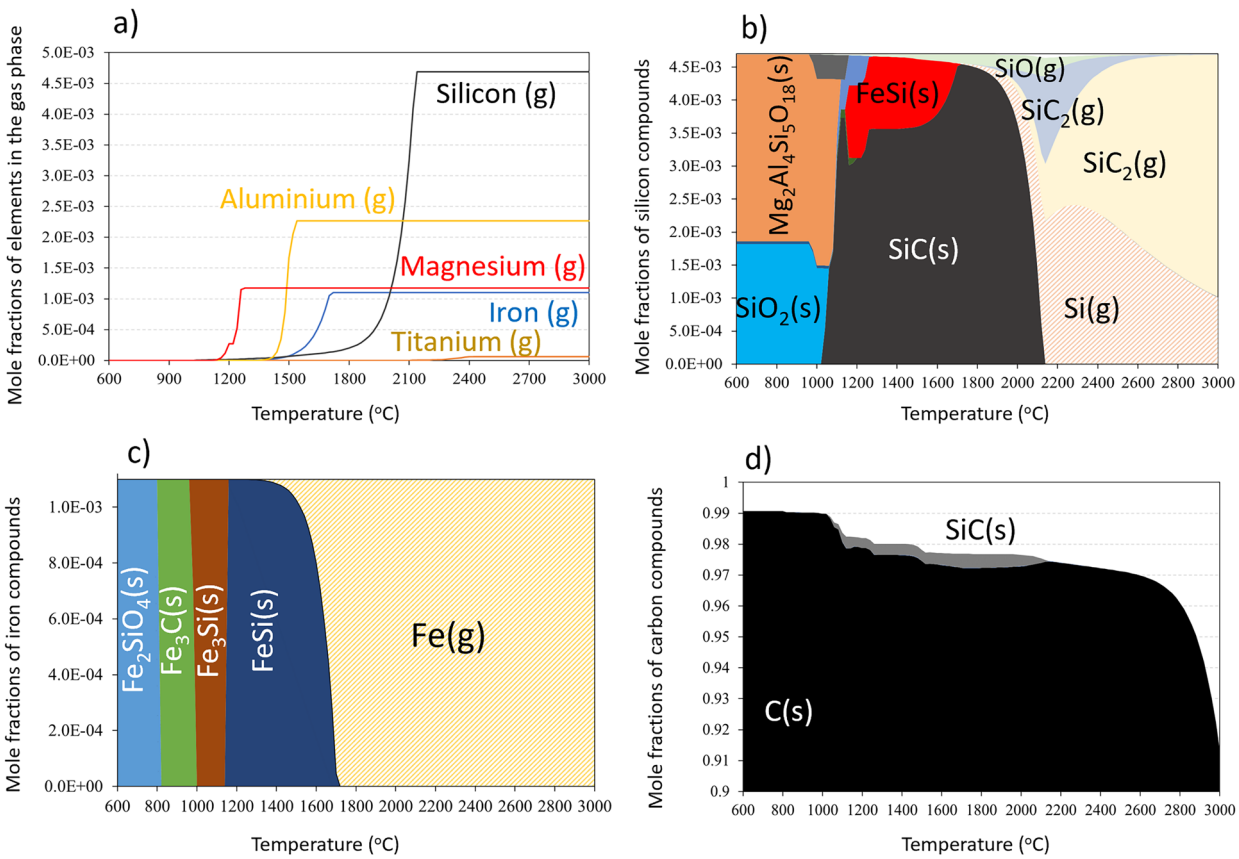

Figure 1: Thermodynamic equilibria of (a) total amount of major gaseous components, including (b) silicon, (c) iron, and (d) solid phase carbon compounds in the flotation purified graphite.

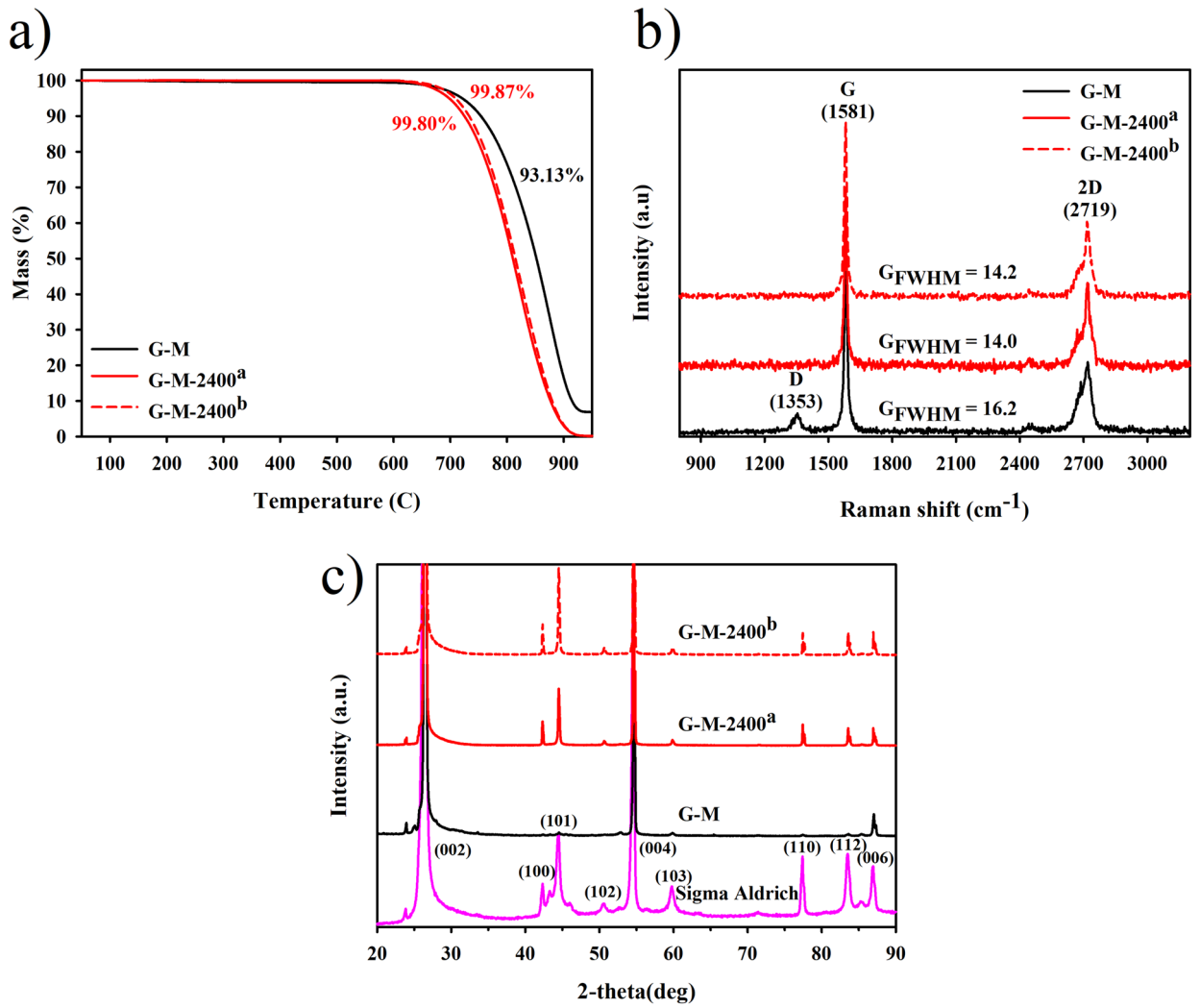

Figure 2: (a) The thermogravimetric analysis and (b) Raman spectra and (c) XRD of Sigma-Aldrich graphite, G-M, G-M-2400a (1st batch) and G-M-2400b (2nd batch).

as identified by SEM/EDS mapping (Fig. S1) and ICP-MS, see Table 1. The thermal treatment at 2400 °C significantly improved the purity of the samples (G-M-2400) and the observed mass loss in the TGA was increased up to 99.8% while the remaining mass of impurities was only around 0.2%.

The high temperature treatment time (below 15 min) used for the purification in the studies is relatively short time compared, for example, to the production of synthetic graphite, which is typically produced at temperatures between 2500 and 3000 °C and holding time of several hours [9, 10]. The induction heating is also a very efficient high temperature process since its transferable heat is over several times greater compared to the conventional joule heating [12]. In addition to good efficiency and shorter process time, the high temperature thermal treatment also enables the reduction of strong chemicals, such as acids, used in the process obtaining battery grade graphite with high purity and crystallinity [13].

Crystallization and reduction of defects at high temperature thermal treatment

Figure 2 shows the Raman and XRD results of graphite samples before and after the thermal treatment. Natural graphite is typically highly anisotropic, which may decrease the electrochemical performance [14]. Based on the Raman and XRD analysis, the high temperature (2400 °C) treatment not only purified the sample, but it also increased the crystallinity [Fig. 2(c)] and reduced the number of defects in the sample [Fig. 2(b)]. The Raman spectra showed strong G peak at 1582 cm^{-1} in Fig. 2(b), which is due to bond stretching of sp^2 atoms in rings and chains while the two component 2D peak at 2720 cm^{-1} is a characteristic band present in graphite materials. The small D peak at 1351 cm^{-1} was present only in the non-thermally treated sample (G-M) and is due to breathing of sp^2 atoms in rings. D peak typically indicates in-plane defects [13, 15, 16], which can have a negative impact on the electrochemical performance of the graphite.

The samples treated at 2400 °C (G-M-2400) did not display a D peak, and had also lower G_{FWHM} values (14.0, 14.2 cm^{-1}) compared to non-thermally treated graphite (16.2 cm^{-1}). The G_{FWHM} value reflects surface crystallinity, a value around 40 cm^{-1} indicated the presence of turbostratic structure, while values bellow (< 20 cm^{-1}) obtained for G-M-2400 samples are typical for graphite and reflect crystal growth and decrease in d_{002} spacing [17]. This indicates that heat treatment of the natural graphite can improve the powder properties such as crystalline structure that are important for their electrochemical performance in the LIBs.

The crystallinity of the samples before and after the thermal treatment was compared to commercial graphite (Sigma Aldrich) by using XRD analysis. Aitolampi graphite obtained after the flotation treatment was composed mainly of 2H graphite (PDF 01-071-3739) and displayed reflections (00*l* and *hkl*) indicating 3-dimensional order. The diffractogram from the G-M sample was dominated mostly by reflections from (00*l*) planes, i.e., (002), (004), (006). After heat treatment, both batches G-M-2400a and b displayed even more prominent (hkl) reflection such as (101), (102), (110), and (112), which are related to a higher order 3-dimensional crystallinity [18]. The interplanar d_{002} spacing for both G-M and G-M-2400$^{a/b}$ samples was 0.335 nm (and 0.336 nm for Sigma Aldrich) as determined from XRD. These observations are in good agreement with the Raman analysis indicating the increased crystallinity after treatment.

Figure 3 shows the lower (left side) and higher (right right) magnification SEM images of the Sigma-Aldrich (SA) graphite used as a reference, and G-M and G-M-2400 graphite samples. All samples were visually indistinguishable showing typical graphite morphology—layered sheet structures (flakes) that are flat, folded, split, or twisted. The G-M and G-M-2400 samples displayed flake sizes up to 150 µm while the commercial graphite up to 50 µm. There were no significant differences between different batches (G-M-2400 a and b) prepared under same conditions confirming the good reproducibility of the process. Furthermore, the SEM/EDS analysis of G-M and G-M-2400 samples show the reduction of the main impurities from the powder (see Supplementary Fig. S1), which is in good agreement with ICP-MS analysis.

Electrochemical performance of G-M and G-M-2400 graphite powders

Electrochemical performance of thermally treated G-M-2400 graphite powder was investigated in the half- and full cells for LIBs and compared with non-thermally treated G-M powder. Figure 4 shows voltage profiles for the first and 4th cycles. Typical three intercalation stages for the graphite can be clearly seen as voltage plateaus between different phase transition stages [19]. Graphite anodes were first discharged with low current of 0.01 C and SEI (solid electrolyte interface) layer formation can be seen as capacity (mAh/g) over the 0.2 V vs. Li/Li^+ in Fig. 4(a), most of the SEI layer formation takes place between 0.8 and 0.2 V vs. Li/Li^+ [20]. The G-M-2400 sample shows lower level of SEI layer formation indicating that surface area is reduced during the heat-treatment. Table 2 shows that specific capacities are higher for the G-M-2400 and can explained by the lower level of impurities detected with ICP-MS as shown in Table 1. The coulombic efficiencies of the 1st and 4th cycles were higher for G-M-2400. The improved material properties with higher level of crystallinity and reduced the number of defects in graphite structure (Fig. 2) obtained by the fast high temperature annealing can explain the reduced irreversible SEI layer formation and a more reversible Li intercalation process inside graphite. Later, these results will be confirmed by better capacity retention for the longer cycling tests in full cell application.

DC discharge capacity, *CC* charge capacity.

Table 3 shows specific capacities of the full cells formation and rate performance cycles, which are in good agreement with the half-cell performance. Formation cycle charge capacity of 377.3 mAh/g is over theoretical capacity 372 mAh/g, which can be explained by the formation of SEI layer at low current of 0.03 C. In addition, the prepared cell was specifically balanced to achieve high capacity for the anode material. Capacity ratio of the anode/cathode was 0.97 and 1.00 for the G-M-2400 and GM cells calculated with 230 mAh/g theoretical capacity of cathode material and 372 mAh/g for the anode material. Rate performance is quite similar for the samples, delivering good capacity 287.7 mAh/g and 277.4 at 1 C for G-M-2400 and G-M, respectively. The voltage profiles in Fig. 5(b) show slightly higher voltage at the beginning of the discharge cycle for G-M which can be explained by its higher surface area. It is well known that graphite with a higher surface area can result in better high-rate tests compared with reduced surface area graphite [20]. Figure 5(a) shows full cell cycling data at 1 C until 600 cycles and capacity check cycles at 0.2 C every 100 cycles. At the beginning of the tests G-M-2400 showed 15.5 mAh/g higher specific capacity (compared to G-M) and after 600 cycles the difference increased up to 40mAh g-1 indicating much better reversibility of Li-ion intercalation process due to the heat-treatment, which is due to higher level of crystallinity and reduced number of defects (see Fig. 2) of the thermally treated G-M-2400 samples. The difference in capacity at the beginning of the tests can be explained by lower level of impurities of the G-M-2400 samples compared to the non-treated G-M samples and by the small differences in the anode/cathode capacity ratio of the samples.

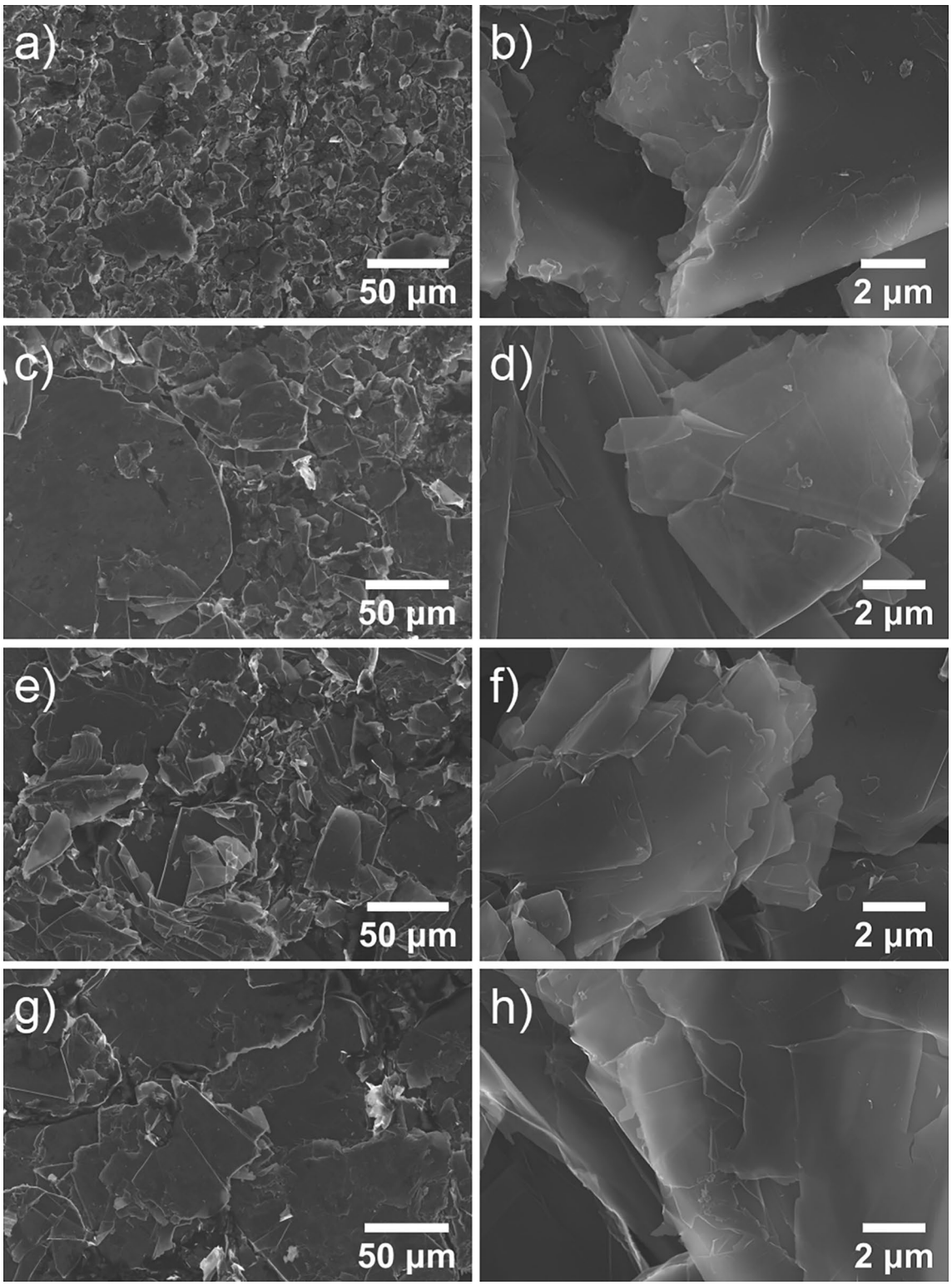

Figure 3: SEM of (a, b) Sigma Aldrich graphite, (c, d) G-M, (e–f) G-M-2400a (1st batch) and (g, h) G-M-2400b (2nd batch).

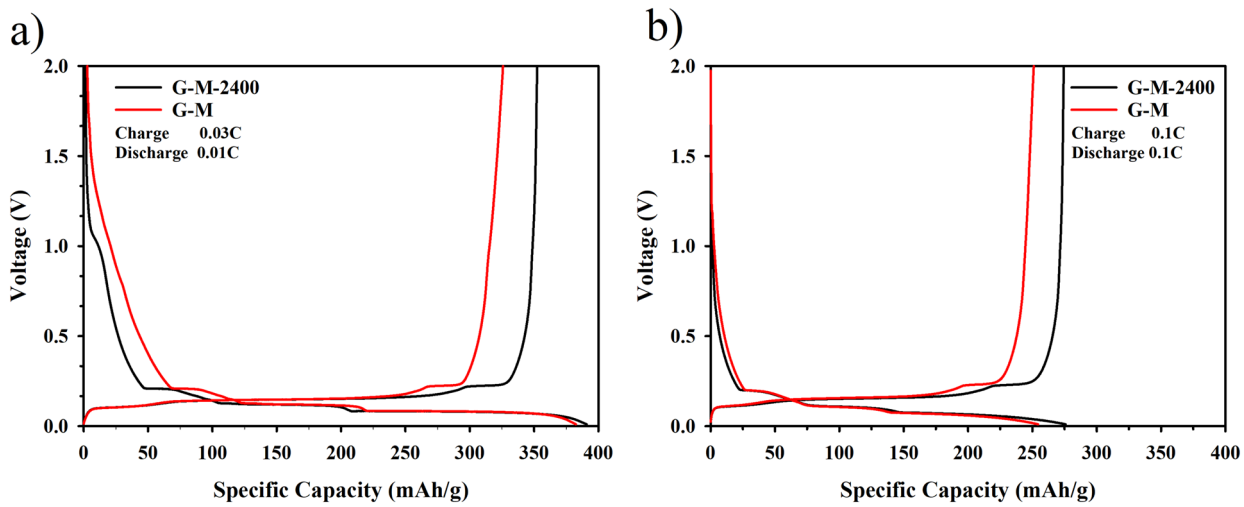

Figure 4: Voltage profiles of prepared samples. (a) Discharge at 0.01 C and charge at 0.03 C. (b) Discharge at 0.1 C and charge at 0.1 C.

TABLE 2: Half-cell performance of two parallel cells for untreated (G-M) and heat-treated sample (G-M-2400).

Samples	1st cycle (mAh/g)			4th cycle (mAh/g)		
	DC 0.01C	CC 0.03C	Eff (%)	DC 0.1C	CC 0.1C	Eff (%)
G-M	375	330.3	88.1	255.3	253	99.1
G-M	382.5	325.8	85.2	254.5	251.1	98.7
G-M-2400	390.5	347.9	89.1	274.7	273.2	99.4
G-M-2400	390.8	352.4	90.2	275.9	274.4	99.5

TABLE 3: Full cells formation and rate performance cycles.

C-rate charge/discharge	Formation and rate performance cycles							
	0.03/0.1 C	0.2 + 0.03/0.2 C	0.2 + 0.03/0.5 C	0.2 + 0.03/1 C	0.2 + 0.03/2 C	0.2 + 0.03/3 C	0.2 + 0.03/5 C	0.2 + 0.03/10 C
G-M-2400 charge mAh/g	377.3	326.1	314.3	300.2	288.5	273.6	259.5	231.8
G-M-2400 discharge mAh/g	326.8	316.5	300.1	287.7	272.2	258.0	230.4	143.6
G-M charge mAh/g	358.6	309.3	297.9	288.9	277.9	261.7	246.2	219.3
G-M discharge mAh/g	310.3	301.0	288.3	277.4	261.0	245.5	218.3	121.1

Heat-treated (G-M-2400) and non-heat treated (G-M) samples.

Conclusion

In this work, high temperature thermal purification of natural graphite originating from the Aitolampi deposit (Finland) was carried out by induction annealing. The non-treated graphite samples contained several impurities, such as Na, Mg, Al, Si, K, Ca, Fe, Zn, V with initial impurity concentrations in the range of 10 000 µg/g–70 000 µg/g based on the ICP-MS analysis. The pre-treatment of the samples with flotation increased the graphitic carbon content and decreased the individual contaminant concentration below 10 000 µg/g. However, the purity and carbon content of the sample was still only around 93.1 wt%. The purity was greatly increased above 99.8% with a 15 min thermal treatment at 2400 °C carried out by using induction annealing in Ar atmosphere at atmospheric pressure. The flotation combined with induction annealing had a significant impact in removal of the most prominent impurities. The concentrations of impurities such as Na and Si decreased below the detection limit, Mg, Zn, and V below 100 µg/g, Al, Na, and Ca below 1000 µg/g. Furthermore, the Fe content was three times lower than the Fe content after only flotation treatment. In addition, thermal treatment was observed to create higher order 3-dimensional crystallinity, which is an important parameter related to the electrochemical performance of graphite in the LIBs.

Overall, the electrochemical results were better for the thermally treated graphite due to an improved purity and higher crystallinity with less defects in structure which resulted in less

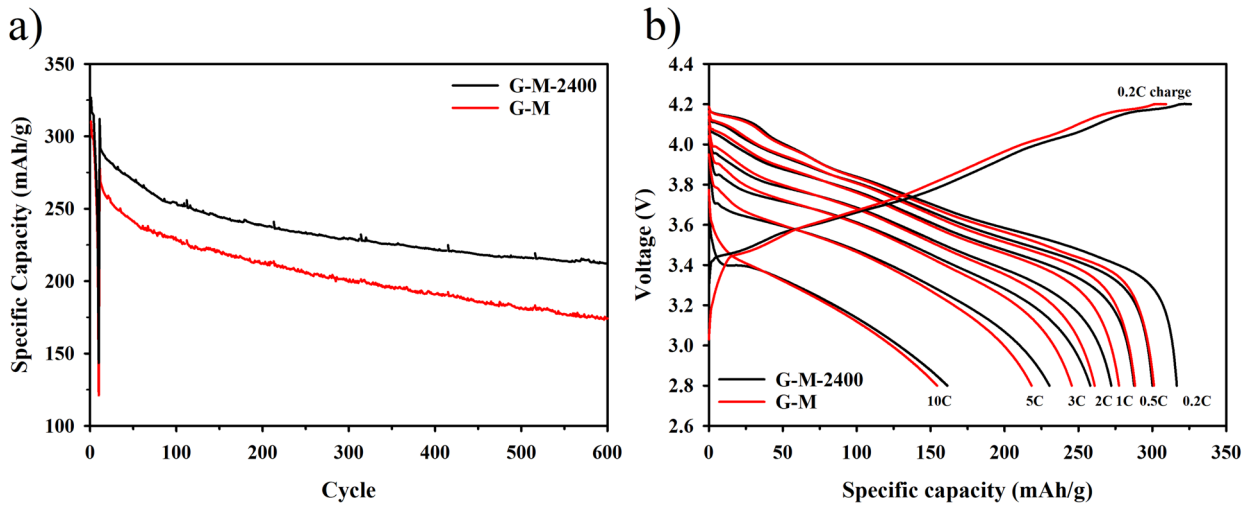

Figure 5: (a) Cycle vs. specific discharge capacity, (b) voltage profiles at different rates of full cell for the heat-treated G-M-2400 and untreated G-M cells.

SEI formation and a more reversible Li^+ intercalation process. The remaining iron impurities did not have significant effect on the electrochemical performance. Full cell test shows that the thermally treated graphite, G-M-2400, had superior performance compared to graphite, which was only purified with the flotation, G-M. The G-M-2400 graphite achieved an initial capacity of 291.8 7 mAh/g at 1 C discharge current, while G-M remained at 268.9 mAh/g. In cycling stability, the G-M-2400 retained 73% of its specific capacity after 600 cycles, compared to 65% for G-M.

Materials and methods

Properties of the graphite samples used for the thermal treatment

Natural graphite was provided by Grafintec, Finland. It originated from Aitolampi deposit, and a mid-fraction of the sample was used. Based on the earlier mineralogical study of GTK [21, 22], graphite deposits in high metamorphic terrains in Finland have typically a flaky-like morphology consisting commonly of biotite, quartz, feldspar, chlorite, and Fe-sulfides. The graphite flakes were found to range in size from 50 to 1600 µm, with the majority being between 200 and 500 µm in length, and the ratios between their long and short axes were in the range of 2 to 5 for most of the flakes. The average of the indicated graphite content in Aitolampi formation is 5.1 wt-% (TGC, total graphitic carbon) with a total sulfur 5.0 wt-% (https://www.grafintec.fi/aitolampi/).

The graphite flakes were pre-purified by conventional flotation and divided into fine (< 75 µm), medium (75–180 µm), and large (> 180 µm) fractions [21, 22]. The obtained graphite concentrates still contained mineral impurities indicating that additional purification processes were still needed to reach the battery grade graphite. The medium fraction was selected to be used in the studies as it is in the size range typically used in electrochemical applications. Shortly, flotation of graphite typically includes generally a rougher flotation and followed 3–6 cleaning stages [23]. Graphite is a hydrophobic mineral, applied flotation chemicals are MIBC (Methyl Isobutyl Carbinol) as a frother, Na_2SiO_3 and Starch as a depressant. Even hydrophobic solids attach easily to the surface of gas bubbles rising through suspension, kerosene is commonly added as a collector [24]. Alkaline conditions, set up with NaOH (pH > 9), enhance floatability of naturally water-repellent graphite [25]. Among processing sites lacking fresh water, which is generally utilized in flotation cell, enriching of graphite is also workable in the presence of dissolved salt ions (saline water), also according to test experiments of inorganic salts, including potassium chloride (KCl), magnesium chloride ($MgCl_2$), and aluminum chloride ($AlCl_3$) in [26]. Before flotation, graphite ore is crushed and further grinded with ball and rod mills, in cases (related to ore type) also in two stages, firstly for obtaining big flakes of over 100 mesh (> 147 µm) and the second stage to liberate finer fractions for the final flotation [27].

Thermal treatment

Induction annealing of medium sized graphite flakes (75–180 µm) and a pristine graphite (raw ore) sample without pre-treatment was carried out at 2400 °C in argon (AGA 5.0) atmosphere at atmospheric pressure for 15 min, see Table 4. The detailed description of the set-up and operation principles of the induction furnace have been provided elsewhere [28]. Shortly, different batches of equal mass (around 5.0 g) were placed in the graphite crucible that was heated with the 35 °C/min ramp

TABLE 4: Identification of the samples and their treatment processes.

Sample	Pre-treatment	Thermal treatment [°C]
G	n.a.	n.a.
G-M	Flotation	n.a.
G-2400	n.a.	2400
G-M-2400 batch a and b[a]	Flotation	2400
Sigma-Aldrich graphite	n.a.	n.a.

[a]Two batches produced for comparison in same conditions for analysis.
n.a. = not applicable.

up to 2400 °C. The temperature was monitored with an infrared pyrometer (Kleiber 730-LO) with a measurement range from 305 to 2600 °C. The temperature was calibrated with an empty crucible before the experiments. The isotherm at 2400 °C was set to 15 min based on the studies with the large flake fractions of Aitolampi graphite (see supplementary, ST1) and thermodynamic equilibrium calculations described in "Electrochemical performance of G-M and G-M-2400 graphite powders" section. After the isotherm, the sample was cooled down and collected from the furnace.

Thermodynamic equilibrium calculations

Thermodynamic equilibrium calculations were carried out with the Equilib-module of the FactSage 8.0 software to estimate the thermal properties of the impurities in the flotation-treated Aitolampi natural graphite and their vaporization during heating. The module uses the method of Gibbs energy minimization to calculate equilibrium conditions for given multicomponent systems [29] in this case heating of graphite in argon flow. Thermodynamic data of the condensed and gas-phase species were taken from the FactPS and FToxid databases. The elements included in the calculations were C, Si, Mg, Fe, Al, Ti, O, and Ar. Only impurities with concentrations above 200 mg/kg, based on the ICP-MS analyses of the flotation-treated graphite (G-M), were considered in the calculations. The amount of oxygen was calculated based on the oxide form of the impurities. Since the graphite sample is surrounded by continuous argon gas flow during heating, the equilibrium was calculated at argon-graphite molar mixing ratio of 5:1. The calculation was carried out at a pressure of 1 bar and temperature range of 300–3000 °C. It should be noted that the equilibrium results present theoretical estimates for perfectly mixed systems and do not consider imperfect mixing and kinetic limitations in the chemical reactions. Nevertheless, thermodynamic equilibrium often gives plausible estimates on partitioning of inorganic chemical components at high temperature multicomponent systems.

TABLE 5: Coin cell testing program.

Cycle number	1	2	3	4
Discharge C-rate	0.01	0.03	0.03	0.1
Charge C-rate	0.03	0.03	0.03	0.1
Voltage range (V)	0.005–2.0	0.005–2.0	0.005–2.0	0.005–2.0

Characterization

The elemental composition of pristine, untreated graphite flakes, and induction annealed samples were analyzed with the inductively coupled plasma spectrometer (ICP-MS Perkin Elmer Elan 6000). The thermogravimetric analysis (TGA, Q50, TA instruments) of the samples were carried out in air atmosphere. The crystallinity and crystalline phases were analyzed with the x-ray diffraction (XRD, Bruker AXS D8 Advance, Bruker) using CuK_α radiation (40 kV, 40 mA) in the 2θ-range from 10 to 100° and a step size of 0.03°. Raman spectroscopy (Thermo DXR2xi Raman) was carried out at wavelength 532 nm to analyze the composition and defects of the samples. The morphology and structural analysis of the samples before and after the thermal treatment were carried out with the scanning electron microscope (SEM, Zeiss Sigma HDVP) coupled with an energy-dispersive X-ray spectroscope (EDS, Thermofisher). SEM & XRD analysis included a commercial reference graphite (Sigma-Aldrich, USA). Particle size was measured using laser diffraction particle size analyzer (Malvern Mastersizer 3000). In the calibration of the device, the reference sample was used. Tapped density was measured according to the standard measurement using instrument (ERWEKA SVM 222) with stroke high of 3 mm and number of strokes 3500.

Cell assembling and electrochemical characterization

Electrochemical performance testing was conducted using both half-cells, with metallic lithium as the counter electrode, and full cells, with $LiNi_{0.88}Co_{0.9}Mn_{0.3}O_2$ (NCM) as the cathode material. All electrode foils and battery cells were prepared in dry room conditions. An anode slurry was mixed using a mixer (Thinky ARE-250). The slurry composition was 4% polyvinylidene fluoride (Kureha #9300), 4% carbon (Timcal C45), and 92% active material, with 1-methyl-2-pyrrolidinone (Alfa Aesar, anhydrous 99.5%) as a solvent. The slurry was spread on copper foil with 200 µm applicators before being dried on a hot plate at 50 °C for a one hour and finally being placed in a vacuum oven at 80 °C overnight. The anode foil was calendared before cell assembly. The active material loading on the foil was about 2.5 mg/cm^2. Two 2016-type coin cells were assembled from each sample foil with metallic lithium as the counter electrode and 1.15 M $LIPF_6$ in EC:DMC:EMC (2:4:4), and 1% vinylene carbonate as the

electrolyte. Cells were cycled four times at 25 °C (see Table 5 for the C-rate used). Cells were at first discharged at a constant current until 0.005 V was reached, and after that charged at a constant current until 2.0 V was reached. Cells were tested at 25 °C. The theoretical capacity used to calculate the C-rate was 370 mAh/g.

One electrode pair pouch cell (50 mAh) was prepared with a NCM cathode, an electrolyte of 1.15 M $LIPF_6$ in EC:DMC:EMC (2:4:4), and 1% vinylene carbonate. After the formation and rate performance cycles, the pouch cells were at first charged at a constant current 1 C until 4.2 V was reached, and after that with a constant voltage until the current decreased to 0.03 C and discharged to 2.8 V at 1 C. Every 100 cycles, a capacity check cycle at 0.2 C was run and before the capacity check, the cells were discharged at 0.2 C.

Acknowledgments

Not applicable.

Author contributions

AL: Conceptualization, methodology, validation, formal analysis, data curation, writing—original draft, writing—review and editing, resources, project administration. JV: Investigation, formal analysis, writing—original draft, review and editing. AM: Investigation, visualization, writing—review and editing. TK: Investigation, writing—review and editing. S-MM: Investigation, validation. OS: Investigation, formal analysis, visualization, writing—review and Editing. SL: Resources, writing—review and Editing. UL: Writing—review and editing, resources, funding acquisition. JJ: Writing—review and editing, funding acquisition.

Funding

Open access funding provided by University of Eastern Finland (including Kuopio University Hospital). The authors acknowledge Business Finland for research funding 2021–2024, University of Oulu (BATCircle2.0, No. 44612/31/2020), Geological Survey of Finland (BATCircle2.0, No. 44386/31/2020), University of Eastern Finland (BATCircle2.0, No. 44836/31/2020).

Data availability

The datasets used and/or analyzed during the current study are available from the corresponding author on reasonable request.

Declarations

Conflict of interest The authors declare that they have no known competing financial interests or personal relationships that could have appeared to influence the work reported in this paper.

Ethical approval

The research and related data presented in the paper are not subjected to any ethical concerns as it does not utilize sensitive information or human or animal tests.

Consent to participate

The research, analysis of data and writing has been carried out in accordance with legislation and good scientific practices as well as research guidelines.

Consent for publication

All authors have seen and reviewed the paper and participated in writing process. All authors have given their consent for publication.

Supplementary Information

The online version contains supplementary material available at https://doi.org/10.1557/s43578-024-01282-z.

References

1. B. Kwiecińska, H.I. Petersen, Graphite, semi-graphite, natural coke, and natural char classification—ICCP system. Int. J. Coal Geol. **57**(2), 99–116 (2004)
2. G.R. Robinson, Jr., J.M. Hammarstrom, and D.W. Olson, Graphite (U.S. Geological Survey, 2017)
3. A.D. Jara et al., Purification, application and current market trend of natural graphite: a review. Int. J. Min. Sci. Technol. **29**(5), 671–689 (2019)
4. J.-H. Lee et al., Aqueous processing of natural graphite particulates for lithium-ion battery anodes and their electrochemical performance. J. Power. Sources **147**(1–2), 249–255 (2005)

5. C.-M. Ye, B.-Q. Shentu, Z.-X. Weng, Thermal conductivity of high density polyethylene filled with graphite. J. Appl. Polym. Sci. **101**(6), 3806–3810 (2006)
6. S. ChehrehChelgani et al., A review of graphite beneficiation techniques. Miner. Process. Extr. Metall. Rev.Extr. Metall. Rev. **37**(1), 58–68 (2016)
7. K. Shen et al., Thermal and gas purification of natural graphite for nuclear applications. Carbon **173**, 769–781 (2021)
8. M. Abdollahifar et al., Graphite recycling from end-of-life lithium-ion batteries: processes and applications. Adv. Mater. Technol. **8**(2), 2200368 (2023)
9. S. Huang et al., Carbonization and graphitization of pitch applied for anode materials of high power lithium ion batteries. J. Solid State Electrochem. **17**(5), 1401–1408 (2013)
10. B. Xing et al., Preparation of synthetic graphite from bituminous coal as anode materials for high performance lithium-ion batteries. Fuel Process. Technol. **172**, 162–171 (2018)
11. N.W.B. Balasooriya, Ph. Touzain, P.W.S.K. Bandaranayake, Capacity improvement of mechanically and chemically treated Sri Lanka natural graphite as an anode material in Li-ion batteries. Ionics **13**(5), 305–309 (2007)
12. R. Rudolf, P. Mitschang, M. Neitzel, Induction heating of continuous carbon-fibre-reinforced thermoplastics. Composites A Appl. Sci. Manuf. **31**(11), 1191–1202 (2000)
13. A.R. Kamali, H. Zhao, Electrochemical conversion of natural graphite minerals into carbon nanostructures incorporated with Fe3Si for Li-ion storage application. J. Alloys Compd. **949**, 169819 (2023)
14. M. Yoshio et al., Improvement of natural graphite as a lithium-ion battery anode material, from raw flake to carbon-coated sphere Electronic supplementary information (ESI) available: colour versions of Figs 6, 8 and 9 See http://www.rsc.org/suppdata/jm/b3/b316702j/. J. Mater. Chem. **14**(11), 1754 (2004)
15. A.C. Ferrari, Raman spectroscopy of graphene and graphite: Disorder, electron–phonon coupling, doping and nonadiabatic effects. Solid State Commun. **143**(1–2), 47–57 (2007)
16. A.R. Kamali, J. Feighan, D.J. Fray, Towards large scale preparation of graphene in molten salts and its use in the fabrication of highly toughened alumina ceramics. Faraday Discuss. **190**, 451–470 (2016)
17. A. Yoshida, Y. Kaburagi, Y. Hishiyama, Full width at half maximum intensity of the G band in the first order Raman spectrum of carbon material as a parameter for graphitization. Carbon **44**(11), 2333–2335 (2006)
18. S. Rodrigues et al., Microstructural investigations of natural and synthetic graphites and semi-graphites. Int. J. Coal Geol. **111**, 67–79 (2013)
19. D. Aurbach et al., On the correlation between surface chemistry and performance of graphite negative electrodes for Li ion batteries. Electrochim. Acta **45**(1–2), 67–86 (1999)
20. S.J. An et al., The state of understanding of the lithium-ion-battery graphite solid electrolyte interphase (SEI) and its relationship to formation cycling. Carbon **105**, 52–76 (2016)
21. T. Al-Ani et al., High-grade flake graphite deposits in metamorphic Schist belt, Central Finland—mineralogy and beneficiation of graphite for lithium-ion battery applications. Minerals **10**(8), 680 (2020)
22. T. Al-Ani, Science blog: flake graphite from the high-grade metamorphic Savo schist belt, central Finland: mineralogy and purification of graphite as an anode material for Li-ion batteries. GTK (2021)
23. N. Vasumathi et al., Beneficiation of low grade graphite ore of eastern India by two-stage grinding and flotation. J. Min. Metall. A Min. **50**(1), 9–17 (2014)
24. F.F. Florena et al., Floatability study of graphite ore from southeast Sulawesi (Indonesia), in Jatinangor, Indonesia (2016), p. 050005
25. T. Wakamatsu, Y. Numata, Flotation of graphite. Miner. Eng. **4**(7), 975–982 (1991)
26. Y. An et al., Specific cation effect on the flotation of graphite. Minerals **12**(9), 1070 (2022)
27. L.D. Michaud, Graphite beneficiation process. https://www.911metallurgist.com/blog/graphite-beneficiation-process (2016)
28. A. Meščeriakovas et al., Influence of induction-annealing temperature on the morphology of barley-straw-derived Si@C and SiC@graphite for potential application in Li-ion batteries. Nanotechnology **31**(33), 335709 (2020)
29. C.W. Bale et al., FactSage thermochemical software and databases, 2010–2016. Calphad **54**, 35–53 (2016)